Structure and Dynamics of the Aqueous Liquid−Vapor Interface: A Comprehensive Particle-Based Simulation Study[⊥]

I-F. Will Kuo,*,[†] Christopher J. Mundy,[†] Becky L. Eggimann,[‡] Matthew J. McGrath,[‡] J. Ilja Siepmann,[‡] Bin Chen,[§] John Vieceli,[||] and Douglas J. Tobias[||]

Computational Chemical Biology, Lawrence Livermore National Laboratory, P.O. Box 808, Livermore, California 94551, Departments of Chemistry and of Chemical Engineering and Materials Science, University of Minnesota, 207 Pleasant Street SE, Minneapolis, Minnesota 55455-0431, Department of Chemistry, Louisiana State University, Baton Rouge, Louisiana 70803, and Environmental Molecular Science Institute and Department of Chemistry, University of California−Irvine, Irvine, California 92697-2025.

Received: November 2, 2005; In Final Form: December 9, 2005

This research addresses a comprehensive particle-based simulation study of the structural, dynamic, and electronic properties of the liquid−vapor interface of water utilizing both ab initio (based on density functional theory) and empirical (fixed charge and polarizable) models. Numerous properties such as interfacial width, hydrogen bond populations, dipole moments, and correlation times will be characterized with identical schemes to draw useful conclusions on the strengths and weakness of the proposed models for interfacial water. Our findings indicate that all models considered in this study yield similar results for the radial distribution functions, hydrogen bond populations, and orientational relaxation times. Significant differences in the models appear when examining both the dipole moments and surface relaxation near the aqueous liquid−vapor interface. Here, the ab initio interaction potential predicts a significant decrease in the molecular dipole moment and expansion in the oxygen−oxygen distance as one approaches the interface in accordance with recent experiments. All classical polarizable interaction potentials show a less dramatic drop in the molecular dipole moment, and all empirical interaction potentials studied yield an oxygen−oxygen contraction as the interface is approached.

Introduction

Liquid−vapor interfaces of hydrogen bonding fluids are ubiquitous in nature and in technological applications, yet there remain many unresolved and outstanding questions regarding the microscopic properties of these interfaces. Recent experiments and simulations have extended our knowledge on the structure of the interface between neat water and its vapor. Having a detailed understanding of the chemical, dynamical, and structural properties of the aqueous interfacial systems has far-reaching implications in atmospheric science both in their role in heterogeneous processes as well as resolving the discrepancies in the accommodation coefficients for the uptake of gases in droplets. While the understanding of bulk phases of hydrogen bonding fluids is far from complete, there exists significant motivation to investigate these systems in more complex interfacial environments. For example, the interface of hydrogen bonding fluids with lipids and other hydrophobic materials is central to cell biology.[1−5] Atmospheric scientists would like to better understand heterogeneous chemistry in the presence of an inorganic electrolyte and to resolve the discrepancy in the mass accommodation coefficients for gases at the air−water interface.[6−9] Knowledge of the soil (clay)−water and other substrate−water interfaces are essential to develop improved water purification strategies. Overall, this has led to a surge of activity within the chemical physics community over the past two decades directed toward developing innovative surface-sensitive spectroscopic techniques.[10−22] Some of the most recent experimental findings have revealed unexpected molecular structure and electronic distribution present at liquid−vapor interfaces.[10−22]

Beginning 10 years ago, the first of these advanced surface-sensitive spectroscopic studies, using the sum frequency generation (SFG) technique, provided a detailed experimental picture of the neat aqueous liquid−vapor interface.[15,17−20] These experiments pointed to structure at the interface that was distinct from the bulk. A sharp peak at ∼3700 cm^{-1} indicates the presence of dangling hydrogen bonds at the interface, suggestive of molecules with one free OH bond extending out of the surface. A pronounced shoulder attached to the prominent peak at ∼3400 cm^{-1}, which is absent in spectra for bulk water, indicates the presence of a different interfacial hydrogen bonding arrangement.[17] More recently, X-ray absorption spectroscopic (XAS) investigations, carried out on both bulk and interfacial systems, have challenged the conventional views of the structure of these systems.[11−14,23,24] The XAS results on bulk liquid water have produced a picture of the first solvation shell that remains controversial,[23,24] while studies of liquid microjets consisting of neat water or methanol produced strong evidence for different types of surface molecules at the interfaces.[11−14] For the neat aqueous interface, an "acceptor-only" surface moiety was proposed wherein both hydrogen atoms of a surface water molecule extend out of the liquid.[12] This contrasts the picture

[⊥] Part of the special issue "Michael L. Klein Festschrift".

* Corresponding author. E-mail: kuo2@llnl.gov.

[†] Computational Chemical Biology, Lawrence Livermore National Laboratory.

[‡] Departments of Chemistry and of Chemical Engineering and Materials Science, University of Minnesota.

[§] Department of Chemistry, Louisiana State University.

[||] Environmental Molecular Science Institute and Department of Chemistry, University of California−Irvine.

10.1021/jp056330t CCC: $33.50
Published on Web 01/20/2006

provided by SFG of the well-recognized "single-donor" water that has only one dangling hydrogen.[15−19,25] However, the ability of XAS to distinguish between acceptor-only and single-donor species may not be adequate.[15] The XAS measurements are sensitive to the precise nature of the solvating environment around a reference oxygen atom, whereas the SFG signal is sensitive to changes in vibrational frequencies produced by different hydrogen bonding environments. A somewhat surprising result was observed from extended X-ray absorption fine structure (EXAFS) experiments. Wilson et al. reported outward surface relaxation (expansion) of ∼6% for the aqueous liquid−vapor interface compared to inward relaxation (contraction) of ∼5% for the neat methanol interface.[13,14] This outward relaxation for water is clearly related to charge rearrangement due to the unsatisfied bonding in the vicinity of the interface. Such novel spectroscopic findings have presented a new theoretical challenge, namely connecting these experimental observations to microscopic-level properties of these liquid−vapor interfaces.

In principle, particle-based simulation methods offer an attractive approach to unravel the microscopic details of these surfaces. The first detailed molecular dynamics (MD) calculations of the air−water interface were performed 15−20 years ago by employing empirical pairwise additive potentials (Lennard−Jones and Coulomb interactions with fixed charges) to model liquid water.[26−28] These studies were the first quantitative calculations providing both structural and thermodynamic information about this important system. Although these MD studies predate the advent of sophisticated surface-sensitive spectroscopies, they have provided a template upon which all subsequent MD studies have been based. In response to the SFG experiments, Benjamin computed the surface infrared spectrum of water by using a flexible version of the simple point charge (SPC) model and found remarkable agreement with experiment.[29,30] This MD study was able to qualitatively reproduce the spectroscopic signals for both the existence of dangling OH bonds and the alternative hydrogen bonding arrangement at the surface. Thus, it seems that empirical fixed-charge models for water, despite being parametrized to reproduce bulk structural properties, are able to adequately reproduce structural properties in the vicinity of the liquid−vapor interface as well.

The remaining challenge is to reproduce accurate thermodynamic properties, such as the surface tension, vapor−liquid partitioning, and interfacial adsorption. Polarizable water models are an important next step in answering this challenge, and a substantial amount of effort has been invested in developing models that incorporate the polarization present at the aqueous liquid−vapor interface.[31−33] However, there remain concerns that even polarizable models may not be adequate for capturing all of the fundamental physical chemistry revealed by the recent X-ray data.[10−14,23] A comprehensive study of the air−water interface should include many-body polarization effects in a parameter-free manner through the use of ab initio quantum potential. Models based on density functional theory (DFT) are well suited for condensed phase dynamics studies. Compared to other ab initio methods, DFT maintains relatively high accuracy at modest computational cost, and has previously been unified with a molecular dynamics approach in the work of Car and Parrinello.[34,35]

One of the major limitations of Car−Parrinello Molecular Dynamics (CPMD) and other DFT-based methods is the significantly increased computational expense relative to empirical models. A first attempt at using DFT-based methods to elucidate the aqueous liquid−vapor interface was performed by using 32 water molecules.[36] Although this study provided interesting observations of surface moieties, the system size was not large enough to yield a stable interfacial system. Through the recent availability of tera-scale computing at the Lawrence Livermore National Laboratory (LLNL) and the excellent scaling properties of CPMD,[35,37] some of the authors were able to simulate a stable aqueous liquid−vapor interface with ab initio interaction potentials[38] for a system of 216 water molecules. This simulation provided direct evidence for "acceptor-only" hydrogen-bonded species as well as signatures for the observed surface relaxation.[38]

It is clear from this discussion that there is an abundance of both experimental and theoretical data on the aqueous liquid−vapor interface. In this study, we will present a comprehensive theoretical approach, including both ab initio and molecular mechanics simulations, which will provide a thorough microscopic-level perspective on the structural, dynamic, and electronic properties of this important interface. One of the central goals of this paper is to provide a proper comparison for some of the more popular water solvent models with the data obtained from ab initio calculations. We show results for a selected set of empirical models by using molecular dynamics (MD) and Monte Carlo (MC) simulation techniques. MC is necessary primarily for its robust equilibration (i.e., all degrees of freedom are guaranteed to obey the equipartition theorem) and direct access to thermodynamic data such as saturated vapor pressure and heats of vaporization through the use of the Gibbs ensemble MC method.[39,40] Structural and electronic quantities will be computed via MC by using the extended simple point charge model (SPC/E),[41] the transferable intermolecular potentials-4-points model (TIP4P),[42] and two polarizable versions of the TIP4P model, the so-called fluctuating charge model FLUC-q[31] and TIP4P−POL2.[32] Dynamic quantities will be computed with MD for SPC/E,[41] TIP4P,[42] and POL3,[43] which is a polarizable model. The structural and dynamical properties of the classical water model employed here have been examined throughout literature and are often believed to give faithful representation for different aspects of liquid water. In particular, TIP4P−POL2 is believed to provide the current best benchmark for real-space water structure at biologically relevant temperatures.[44] The structural and dynamic quantities for the DFT-based interaction potential will be computed with the CPMD method. Such an extensive study will enable us to compare and contrast the important aspects of a many-body potential on the structural and dynamic properties of the aqueous liquid−vapor interface within an identical analysis framework. To this end, we will examine the effects of the interaction potential on the interfacial width, bulk, and interfacial structure, dipole moments, hydrogen bond populations, surface relaxation, orientational dynamics, and retention times.

Simulation Details

Car−Parrinello Molecular Dynamics. All CPMD simulations were performed on the 11 teraflop Multiprogrammatic Capability Resource (MCR) Linux cluster at LLNL (see http://www.top500.org). The parallelization of CPMD uses both OpenMP and MPI directives to scale well to a total of 1440 CPUs.[35,37,45] Our simulation parameters were chosen with a fictitious mass of 400 au for the electronic degrees of freedom and a time-step of 0.097 fs. Decoupling of the periodic images (2D) were performed as described by Mortensen and Parrinello,[35,46] and the amount of vacuum (35 Å) was chosen such that this simulation was well converged with respect to this parameter. Gradient-corrected exchange and correlation functionals with the BLYP parametrization were used.[47,48] The

interaction between core and valence electrons are described by Martins−Troullier pseudopotentials.[49] An energy cutoff of 70 Ry was used for the orbitals. Nosé−Hoover thermostats[50,51] were attached to every degree of freedom, with a thermostating frequency of 3800 cm^{-1}, to ensure thermal equilibrium over the entire MD trajectory. The electronic kinetic energy was stable throughout the entire simulation, indicating that our choice of time-step and fictitious electronic mass preserved adiabaticity.[52] All postprocessing of the electronic structure was performed with the CP2K/QUICKSTEP module.[53−55] For analysis, averaging was performed every 15 configurations, selected from the last 4 ps by using the QUICKSTEP module in conjunction with a gradient-corrected BLYP functional,[47,48] dual-space pseudopotentials,[56] and a triple-ζ plus double polarization (TZV2P) basis set for the valence states.[54,57] Our ab initio simulation of the aqueous liquid−vapor interface was performed on 216 waters in a simulation cell of dimension 15 Å (x) × 15 Å (y) × 71.44 Å (z). The distance between the two free interfaces in the z direction was approximately 35 Å, indicating that there should be roughly 5−10 Å of bulk liquid within our water slab. The initial configuration was obtained from classical molecular dynamics after an equilibration period of 100 ps at 300 K. After the initial wave function optimization, CPMD was performed for 7 ps. The analysis presented here is based on the last 4 ps of the CPMD trajectory.

Classical Molecular Dynamics. Classical molecular dynamics (MD) simulations were performed for the SPC/E,[41] TIP4P,[42] and POL3[43] models. Each system consisted of 864 water molecules in a slab configuration with box dimensions of 30 Å (x) × 30 Å (y) × 100 Å (z) and three-dimensional periodic boundary conditions. This box geometry and number of molecules yielded an approximately 25 Å wide bulk liquid region with two independent liquid−vapor interfaces on each side, where the z dimension was perpendicular to the interfaces. The water slab was equilibrated for 500 ps in the NVT ensemble with a 1 ns production run total in the NVE ensemble at an average temperature of 300 K. For the production run, the velocities were resampled every 100 ps from the Maxwell−Boltzman distribution.

The electrostatic interactions were calculated according to the smooth particle mesh Ewald method,[58] where the real-space portion of the Ewald sum and the Lennard−Jones interactions were truncated at 12 Å. The SHAKE[59] algorithm was used to constrain the bonds to their equilibrium values, and a 1 fs integration time step was used. Version 6 of the AMBER software package[60] was used to perform the MD simulations on a Medium Performance Computing Beowulf Cluster at the University of California−Irvine.

Monte Carlo. Interfacial structural properties for the extended simple point charge model (SPC/E),[41] the transferable intermolecular potentials-4-points model (TIP4P),[42] and two polarizable versions of the TIP4P model, the so-called fluctuating charge model FLUC-q[31] and TIP4P−POL2[32] water, were calculated by using Monte Carlo simulations combining the Gibbs ensemble (GEMC)[39,40] and coupled−decoupled configurational-bias (CBMC) techniques.[61,62] The simulation setup for the interfacial calculations is similar to that used previously by some of the authors for studying the vapor−liquid interface of water/1-butanol mixtures.[63] Here, we utilized an elongated liquid box containing initially 1600 water molecules with dimensions 30 Å (x) × 30 Å (y) × 100 Å (z), and a vapor box with initially 100 helium atoms to ensure a constant pressure. In addition to the external pressure and temperature, the MC simulations maintain as constants the overall numbers of water and helium molecules and the interfacial area of the liquid box. The initial configuration of the liquid slab was taken from an independent NVT simulation of a bulk liquid at 298 K with box dimensions 30 Å (x) × 30 Å (y) × 27 Å (z), which yields a liquid density of 1 g/cm^3. The final configuration of this system was replicated in the z-direction to generate a liquid slab with dimensions 30 Å (x) × 30 Å (y) × 54 Å (z). This slab was placed in the center of the liquid box for the GEMC simulations, allowing for approximately 46 Å of vacuum between the two vapor−liquid interfaces after periodic boundaries were implemented. Equilibration of the slab system at 298 K and 1 atm took place through box volume changes (the volume of the vapor box was allowed to change while keeping all cell lengths equal, but the z-dimension of the liquid slab box was allowed to fluctuate), CBMC swap moves of helium and water molecules between the two boxes, rotation and translation of water molecules, and translation of helium atoms. A total of five independent simulations were run, each consisting of more than 5×10^4 MC cycles for equilibration (where one MC cycle consists of $N = 1700$ randomly selected MC moves) and using 10^5 MC cycles for production. Properties were calculated by averaging over all five independent simulations.

The simulation setup for the TIP4P−POL2 model is similar to that used for the SPC/E model, except that the elongated liquid box contains initially 1500 water molecules with dimension 28 Å (x) × 28 Å (y) × 150 Å (z). This choice of system size/box dimension allows us to use directly those equilibrated configurations resulting from previous liquid−vapor interfacial simulations (using the TIP4P force field) as the starting configurations.[63] A total of 32 independent simulations were generated by using different initial configurations. For each of them, quick charge equilibrations were reached through a few hundred Monte Carlo cycles with solely electronic moves. Then it was further equilibrated for more than 10^4 cycles with both nuclear and electronic moves turned on, using the adiabatic and nuclear electronic sampling Monte Carlo (ANES-MC) algorithm, with a judicious choice of $T_{elec} = \infty$ and $R_{elec} = 1$. The production run consisted of 5×10^4 MC cycles.

Results and Discussion

Interfacial Width. The interfacial width was calculated from the MC and ab initio simulations for BLYP, SPC/E, TIP4P, FLUC-q, and TIP4P−POL2. The density profile in the z dimension, $\rho(z)$, was calculated and fit to a hyperbolic tangent function of the form:

$$\rho(z) = \frac{1}{2}(\rho_l + \rho_v) - \frac{1}{2}(\rho_l - \rho_v)\tanh\left(\frac{z - z_{GDS}}{\delta}\right)$$

where ρ_l and ρ_v correspond to the density of liquid water and water vapor, respectively, z_{GDS} is the Gibbs dividing surface (i.e., the z value at 0.5 ρ_l if ρ_v is negligible), and δ is an interface thickness parameter. δ is related to the "90−10" thickness by a factor of 2.1972, which is the distance between the z values at 0.9 ρ_l and 0.1 ρ_l. The parameters that yielded the best fit to the simulated density profiles are shown in Table 1, except for ρ_v because it is on the order of 10^{-7} or less and is taken to be zero. Plots of the raw data and fits to the density profiles are shown in Figure 1. As one can see from Table 1, there is very good agreement among both the empirical fixed-charge and polarizable models for the interfacial widths (δ) and the density (ρ_l). However, there seems to be remarkable deviation for the BLYP description that warrants explanation. As can be seen from Figure 1, the BLYP density profile is dominated by noise.

TABLE 1: Fitted Density Profile Parameters for Aqueous Liquid−Vapor Interface[a]

	BLYP	SPC/E	TIP4P	FLUC-*q*	TIP4P−POL2
ρ_l (g/cm^3)	0.857	0.997	0.999	1.007	0.995
δ (Å)	0.786	1.544	1.567	1.575	1.782
z_{GDS} (Å)	16.10	26.65	28.54	28.11	28.53

[a] The density profile was fitted to $\rho(z) = (1/2)(\rho_l + \rho_v) - (1/2)(\rho_l - \rho_v)\tanh(z - z_{GDS}/\delta)$ with the center of mass shifted to $z = 0$ for the fitting.

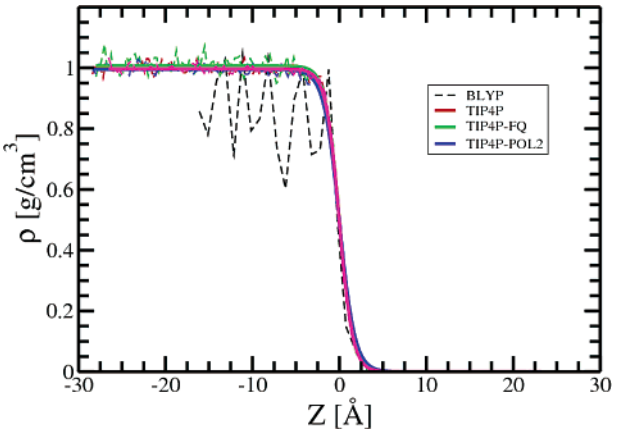

Figure 1. Density profiles for the different water representations. All interfaces are shifted so that the GDS is located at 0.0 Å. The dashed and solid lines show the raw data and their tanh fit, respectively. The fit for BLYP is not shown because lack of good density profile at the interface skews the δ parameter, although the fitted GDS location is used for other property calculations.

This is due to a lack of spatial sampling during the final 4 ps over which the analysis was performed. Thus, any fitting procedure would have to be based on a weighted fit that underscores the uncertainty in the spatial sampling. What remains to be seen (and will be shown later in this manuscript) is whether the BLYP interface is truly converged. However, one salient feature, unambiguously clear from Figure 1, is that BLYP does not reproduce the bulk density of liquid water. If one uses the eye as the interpolator, a density of about ∼0.9 g/cm^3 can be gleaned. In another study, we have performed both GEMC calculations and isothermal−isobaric (*NpT*) MC calculations to ascertain the ambient density of BLYP water.[64−66] Our results indicate that, by using equivalent parameters (in particular, for the charge density cutoff), BLYP has a liquid density of ∼0.9 g/cm^3 at 300 K, which is consistent with results presented here and elsewhere.[38,64−66] Having said this, for the subsequent analysis of the BLYP data in the remainder of the manuscript, we will use an interfacial width parameter (δ) that is the average of those obtained from the empirical models.

Radial Distribution Functions. The radial distribution functions (RDF) for oxygen−oxygen and oxygen−hydrogen pairs (i.e., $g_{OO}(r)$ and $g_{OH}(r)$, respectively) in the interior region of the water slab were calculated for the SPC/E, TIP4P, FLUC-*q*, TIP4P−POL2, and BLYP interaction potential. The interior of the water slab was defined to be a distance of 2δ from the Gibbs dividing surface in order to ensure bulklike properties. As a comparison to experimental RDF for liquid water, we will use TIP4P−POL2 as the benchmark because it is believed that, to date, TIP4P−POL2 provides the current best real-space representation for water structure over biological temperature range.[44] An important observation from Figure 2 is that the first solvation shell of the BLYP interfacial system appears to be somewhat understructured but the deep first minimum suggests that BLYP water is overall more structured then TIP4P−POL2.

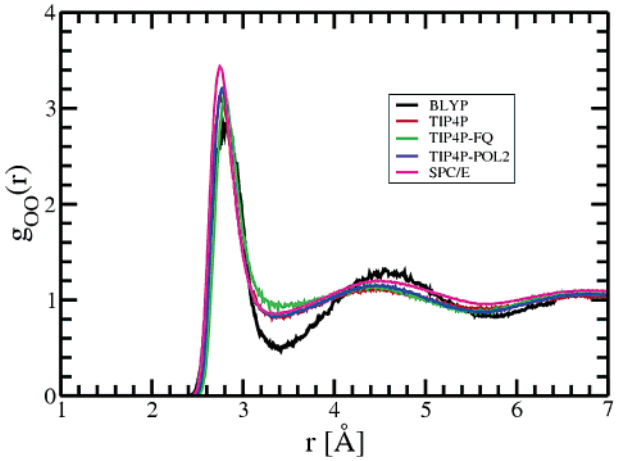

Figure 2. Oxygen−oxygen radial distribution functions in the interior region of the liquid slabs calculated by using a bin width of 0.02 Å.

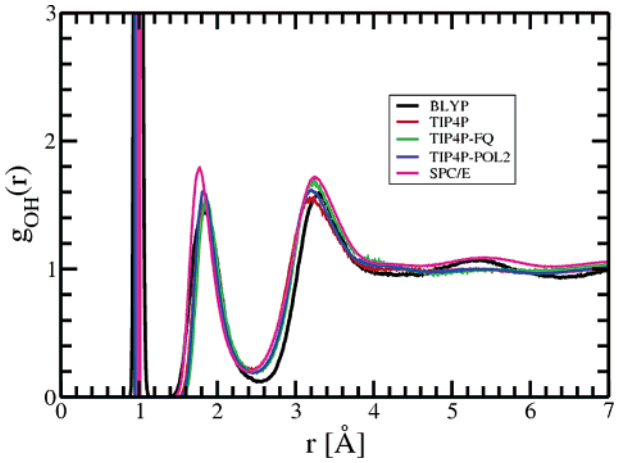

Figure 3. Oxygen−hydrogen radial distribution functions in the interior region of the liquid slabs calculated by using a bin width of 0.02 Å.

It also appears that the SPC/E model produces a significantly more ordered first solvation shell than the other models investigated in this study. Furthermore, the first minimum of the BLYP interaction potential is lower and the second solvation shell is slightly shifted toward larger distances. This behavior was also seen when compared to a BLYP calculation of 64 waters at a fixed density of 1 g/cm^3.[38,52,64,65] This anomaly is most likely due to the fact that the natural density of the BLYP system is different from 1 g/cm^3. It should be noted that the RDFs for the BLYP interfacial system have also been compared to those obtained in an *NpT* ensemble by using MC and the BLYP interaction potential.[65] The RDFs generated by different sampling methods for BLYP water are in good agreement, indicating that the structuring is not an artifact of the interfacial system but rather a reflection of the true density of BLYP water. Similarly, for the oxygen−hydrogen RDFs (see Figure 3), the SPC/E model produces a more ordered structure, while the BLYP water model produces a slightly less structured RDF. For all other water models, the differences in the oxygen−hydrogen RDFs are minimal.

Dipole Moments. Molecular dipole moments computed for the FLUC-*q*, TIP4P−POL2, and the BLYP interactions are plotted as a function of the interfacial depth in Figure 4. The individual dipole moments for the BLYP interaction potential were computed via the Wannier centroid analysis, where the four centers of electron charge (two bonds and two lone pairs) are given a value of $-2e$, reflecting the nature of the spin-restricted calculation.[67,68] It is clear that all models considered

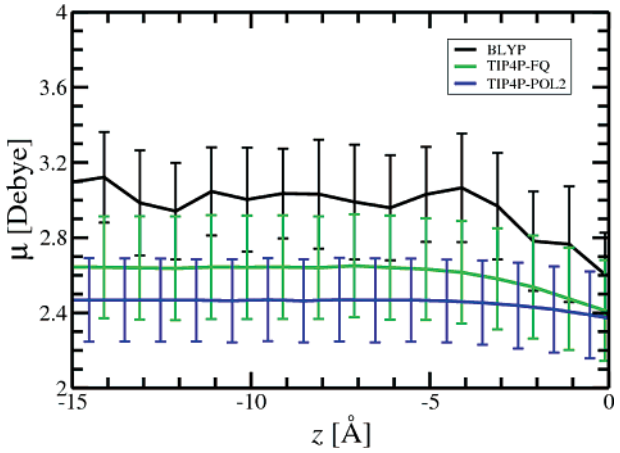

Figure 4. Molecular dipole moment as a function of slab depth. The error bars represent the standard deviation obtained from the dipole moment distribution.

show a drop in dipole moment as one approaches the interfacial region, consistent with the results of Dang and Chang.[33] Furthermore, the dipole moment in the interior of the interfacial slab for the BLYP interaction potential is ~3 D, which is in good agreement with bulk studies using BLYP and indicating that the ab initio interfacial system shows bulk liquid behavior in the interior of the slab.[68,69] Although all models show a decrease in the molecular dipole moment as one approaches the interface, the decrease for the FLUC-*q* and TIP4P−POL2 model is less pronounced than that observed for the BLYP interface. This dramatic loss of the interaction energy in the BLYP model in the vicinity of the interface could account for the surface relaxation.[38]

Hydrogen Bond Populations. There have been recent X-ray experiments that have revealed that an "acceptor only" moiety exists in the vicinity of the interface.[12,14] Although it is beyond the scope of the present article to compute the XAS, particle-based simulations afford the possibility of counting the different hydrogen bonding configurations to compare populations present at the interior and surface of the interfacial system. For this study, four simple hydrogen bond definitions were chosen, ranging from very strict to very loose depending on the choice of angular parameter. The proposed hydrogen bond definition by Wernet et al.[23] is included for completeness. The exact hydrogen bond definitions used are listed in Table 2. Next, each water slab was divided into an "interior" (Table 2) and "surface" (Table 3) region where the "interior" region should exhibit bulklike properties. This division is arbitrary in nature, but we chose a dividing plane in the *xy* dimension, where *z* is 2δ below the Gibbs dividing surface. This is a conservative choice to ensure that the "interior" region of our water slab is minimally influenced by the presence of the interface, which allows for direct comparisons to condensed phased calculations. By using selected hydrogen bonding criteria, we were able to partition each water molecule for a particular region into different species, as characterized by its number of "donor" and "acceptor" hydrogen bonds, where a perfectly tetrahedrally coordinated water will have two "donor" and two "acceptor" hydrogen bonds and designated as (2A, 2D).

In Table 2, the hydrogen bond population for the "interior" of the water slab for each water model is tabulated for the BLYP water model as well as for the four empirical water models obtained from MC simulations. It should be pointed out that the use of different hydrogen bonding criteria will drastically change the hydrogen bonding population for each individual species. Moreover, the use of more restrictive hydrogen bonding criteria will decrease the tetrahedrally coordinated water species (2A, 2D). Last, the Wernet hydrogen bonding criteria produces populations very similar to the least-strict hydrogen bonding definition used in this study.

In Table 3, the hydrogen bond populations at the "surface" of the water slab are tabulated. Unlike the "interior" of the water slab, there is a general trend of deceasing numbers of hydrogen bonds per water molecule going from the "interior" to the "surface", as can be seen by the increased population of less-coordinated species. In addition, all of the different water models tested show qualitatively similar hydrogen bonding populations. For qualitative comparison to experiments, one can deduce the total "single donor" and "acceptor only" populations by summing the 1D and 0D columns, respectively. Thus, any difference in the aforementioned populations at the "surface" versus the "interior" region is evidence of the observed populations that are detected experimentally.[12,19] In our previous study, it was found that there was indeed a distinct population of "acceptor only" hydrogen bond populations present at the surface when compared to the corresponding interior.[38] Likewise, by comparing Table 2 and Table 3, we see that at the "surface", there is an enhanced population of "acceptor only" species as measured by NEXAFS[12] as well as "single donor" species as measured by SFG[17,19] independent of the water model or hydrogen bonding criteria used. In particular, the entries most indicative of the (0D, 1A) "acceptor only" and (1D, 1A) "single donor" populations have a relative increase factor of about 1 and 1.5, respectively. It should be mentioned that the "acceptor only" moiety has not been detected with SFG measurements, and this could be due to many technical issues that are beyond the scope of this paper. However, there have been other independent computational studies that compute SFG spectrum that have identified a surface "wagging" mode for "acceptor only" moieties.[70]

Surface Relaxation. A very interesting phenomena measured by the EXAFS experiment is the surface relaxation in the vicinity of the interface that is manifested as a 6% expansion in the oxygen−oxygen distance in the surface region of the interfacial system.[13] The phenomena of surface relaxation is well-known in solids, where the large surface energy due to unsatisfied bonds is compensated for by a reduction in interlayer spacing as one approaches the solid−vacuum interface. In the case of an aqueous liquid−vapor interface, the surface energy is smaller than a typical solid. Furthermore, the added effect of the water dipole moment decreasing (see Figure 4) in the vicinity of the interface could lead to weaker interactions, and thus, a possible surface relaxation in the form of an expansion. However, quantifying surface relaxation in the case of a liquid is not as straightforward as in a solid, and thus, one must rely on multiple analyses. To this end, in our previous study, we obtained an oxygen−oxygen RDF in the vicinity of the surface as well as a Voronoi[71,72] analysis to confirm the presence of surface expansion in the vicinity of the aqueous liquid−vapor interface.[38] To be able to further quantify the nature of the surface relaxation in the present study, we extend our Voronoi analysis and consider an average oxygen−oxygen distance in both the interior and surface regions in lieu of a surface RDF. The reason for this is that the surface RDF proves to be more difficult for direct comparison between the different models because of the ambiguity in the normalization to the precise density in the interfacial region.

Figure 5 shows both the average and the standard deviation of the Voronoi volume distribution for each individual water molecule as a function of slab depth (zero indicates the location

TABLE 2: Hydrogen Bond Populations (D = Donor, A = Acceptor) for the Interior Region of the Water Slab[a]

BLYP SPC/E TIP4P FLUC-*q* TIP4P−POL2 SPC/E	0D				1D				2D			
0A	6.3	0.8	0.2	0.2	11.1	2.9	1.1	1.0	4.7	2.1	0.9	0.8
	9.3	1.2	0.3	0.2	14.3	4.3	1.4	1.1	5.8	4.3	2.5	2.3
	6.2	1.2	0.5	0.5	11.5	4.0	2.1	2.0	4.9	3.2	2.2	2.2
	6.0	0.8	0.2	0.2	12.3	3.6	1.5	1.3	5.0	3.2	2.1	2.0
	7.4	0.7	0.1	0.1	12.7	3.0	0.7	0.5	5.7	3.5	1.7	1.4
1A	12.0	3.5	1.5	1.4	26.7	19.3	13.7	13.9	13.6	19.8	18.4	18.4
	15.4	5.5	2.2	1.9	25.3	21.0	13.9	12.9	10.6	20.9	22.3	22.1
	10.5	3.5	1.7	1.7	25.5	19.0	14.3	14.3	13.4	18.7	18.8	18.7
	11.8	3.5	1.4	1.2	27.7	21.2	15.1	14.7	12.7	20.2	20.7	20.6
	14.4	4.6	1.7	1.6	26.4	19.9	12.2	11.9	12.2	22.2	22.4	22.3
2A	4.6	2.2	1.0	0.9	12.8	18.3	16.5	16.4	8.1	30.8	45.8	46.1
	5.1	3.6	2.0	1.8	9.6	17.0	16.6	16.2	4.5	20.9	36.1	38.7
	4.1	1.8	0.9	0.8	13.6	16.8	14.9	14.9	10.0	29.6	40.8	41.1
	4.4	2.1	0.9	0.8	12.6	18.2	16.9	16.7	7.3	25.7	38.3	39.5
	5.0	3.1	1.6	1.5	10.5	17.4	15.8	15.7	5.5	24.2	40.7	41.9

[a] The boundary between "interior" bulk water and "surface" water is defined by an arbitrary plane in the *xy* dimension at $z = 2\delta$ below the Gibbs dividing surface. This conservative choice will ensure that the computed hydrogen bond population at the interior of the water slab will have no residual effects caused by the presence of the interface that allows for direct comparison to condensed phase simulation. For BLYP, δ value (1.61 Å) was taken to be the average of the values obtained for the classical empirical interaction potential (see text). For each hydrogen bonding species (i.e. [0D, 0A], [0D, 1A], etc...), the four different columns represent different hydrogen bonding criteria used with the most strict criteria in the leftmost column. From left to right, the hydrogen bonding criteria are: 160° for the angular cutoff (angle formed by the O−H bond vector and the vector from the acceptor oxygen to the donor hydrogen) and 2.27 Å for the distance cutoff (between the oxygen acceptor and hydrogen donor atoms), 150° for the angular cutoff and 2.27 Å for the distance cutoff, 140° for the angular cutoff and 2.27 Å for the distance cutoff, and finally, those proposed by Wernet et al.[23] The angle is defined as the O−H−O angle, and the distance is the intermolecular hydrogen−oxygen distance.

TABLE 3: Hydrogen Bond Populations for the Surface Region of the Water Slab[a]

BLYP TIP4P FLUC-*q* TIP4P−POL2 SPC/E	0D				1D				2D			
0A	13.9	3.5	1.7	1.7	17.8	8.3	4.5	4.5	3.5	2.3	1.1	1.0
	14.8	3.2	1.1	0.9	16.9	7.5	3.6	3.1	4.8	4.1	2.7	2.3
	12.9	4.1	2.3	2.3	16.5	8.8	5.9	5.7	3.6	2.5	1.8	1.8
	9.6	1.9	0.7	0.6	15.9	6.7	3.6	3.2	3.6	2.4	1.5	1.5
	12.1	2.0	0.5	0.4	16.3	5.9	2.2	1.8	4.7	3.6	1.9	1.6
1A	17.3	8.4	5.3	5.0	27.3	34.2	33.3	34.1	7.2	14.8	17.1	16.8
	18.8	9.9	5.7	5.3	24.1	28.0	24.8	24.3	7.5	17.4	21.2	21.6
	15.4	8.1	5.5	5.4	27.5	31.1	30.0	30.1	8.2	14.6	16.4	16.5
	15.2	6.2	3.3	3.1	30.6	33.4	30.6	30.6	8.8	16.3	18.5	18.7
	18.1	8.6	4.5	4.3	26.6	29.2	25.0	25.1	8.3	18.8	22.1	22.4
2A	3.3	2.2	1.2	1.1	6.8	13.8	15.2	15.1	2.9	12.5	20.3	20.4
	4.0	3.5	2.4	2.2	6.5	13.9	16.1	16.1	2.4	12.1	21.5	23.0
	3.0	1.8	1.1	1.0	8.6	13.9	14.9	15.0	4.3	14.6	21.2	21.2
	3.3	1.8	0.9	0.8	8.9	15.8	17.2	17.3	4.0	15.0	22.6	23.3
	3.9	3.0	1.8	1.7	7.1	14.7	16.6	16.6	2.8	13.6	24.2	25.1

[a] The criteria for "interior" versus "surface" water is defined in Table 2. Surface populations for species such as "acceptor-only" (0D column) or "single-donor" (1D column) species are enhanced with respect to the interior counterparts.

of the Gibbs dividing surface). First, it is clear that the Voronoi analysis produces a much smoother profile than the density profile in Figure 1. (This is simply the case because multiple molecules are found and averaged over in each *z*-bin in every snapshot, whereas there is only one data point for the density. Furthermore, the Voronoi volumes relax as any molecule in the Voronoi neighborhood moves, whereas the density requires motion of a specific molecule.) Second, the ab initio BLYP interface is stable, i.e., the average Voronoi volume is flat and the profile is similar to those obtained from the classical empirical interaction potentials. If one looks at the standard deviation of the Voronoi volumes as a function of slab depth, some differences appear. It is clear that, within the interior of the interfacial system, volumes are identical within the standard deviations of all potentials. This points to a picture where the interior density is stable and the volumes fluctuate about a well-defined average (being slightly larger for the BLYP interaction potential). However, as one approaches the interface, the fluctuations about the average volume are distinctly larger for the BLYP representation than those corresponding to classical empirical interaction potentials. This can be interpreted as the onset of an expansion or contraction at the surface.

Although the use of Voronoi analysis is a good indicator of surface expansion, a drawback of this method is that interfacial waters are not accurately described. A more robust method to quantify surface expansion is to compute the average oxygen−oxygen distance in the interior and surface regions of the interfacial system. For the computation of the average oxygen−oxygen distance, we use a cutoff of 3.5 Å as the distance for our search criteria. We find all oxygen−oxygen distances within

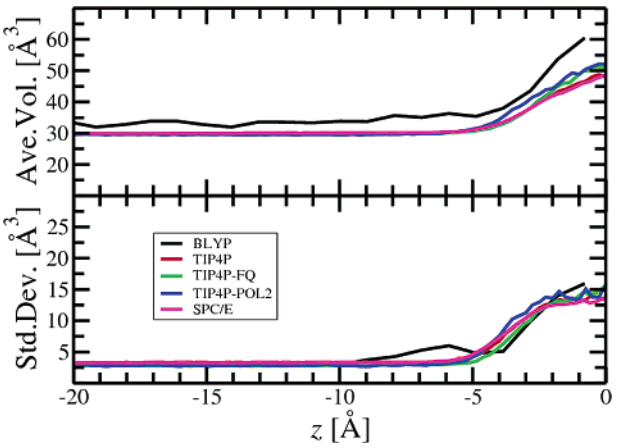

Figure 5. Computed average Voronoi volume per water molecule (top) and standard deviation for its distribution (bottom). A drawback of the Voronoi tessellation method is that interfacial waters are not accurately described. Hence, the average volume has to go up toward the interface.

TABLE 4: Average Oxygen−Oxygen Distance (Å) for Different Water Models in the Interior and Surface Region of the Interfacial System[a]

	$\langle r_{OO}\rangle_{interior}$	$\langle r_{OO}\rangle_{surface}$
BLYP	2.93	2.96
SPC/E	2.95	2.93
TIP4P	2.96	2.94
FLUC-*q*	2.99	2.98
TIP4P−POL2	2.96	2.93

[a] The boundary between interface and interior is taken to be at 2δ below the Gibbs dividing surface. Again, for the case of BLYP, the value of δ used is the average value of classical empirical interaction potential.

this cutoff distance and take the average. Next, the boundary between "interior" and "surface" regions is drawn arbitrarily at 2δ from the Gibbs dividing surface and removes any interfacial effects for the "interior" but at the cost of possibly underestimating surface relaxation phenomenon for the outermost "surface" region. The results are reported in Table 4. Error estimation using block averages that requires each block be statistically independent of other blocks could not be performed due to the length of the BLYP trajectory. It is interesting to note that all the classical empirical potentials point to a decrease of the average oxygen−oxygen distance in the surface region as compared to the interior of the water slab, while the BLYP interaction potential shows an increase in the oxygen−oxygen distance in the surface region pointing to another signature for surface expansion as was measured by EXAFS experiments.[13] It is also worth pointing out that the TIP4P−POL2 model shows the most decrease in the surface oxygen−oxygen distance. This can be understood by noting that the TIP4P−POL2 model uses a breathing Lennard−Jones radius to reflect the amount of charge present at the oxygen site. The decrease in dipole moment (see Figure 4) leads to a decrease in charge that is reflected in a smaller Lennard−Jones radius for the oxygen site.[32] Thus, the present analysis is able to capture this feature of the TIP4P−POL2 model.

It should be noted that our decrease/increase in oxygen−oxygen distance in the surface region for different water models is ∼1%, which is substantially smaller in magnitude then the ∼6% detected in EXAFS experiment. This discrepancy in magnitude could be due to the fact that EXAFS is measuring the surface relaxation normal to the interface, while our oxygen−oxygen distance analysis has no directional bias, and thus, would underestimate the magnitude surface relaxation normal to the interface.

TABLE 5: Interfacial Residence Times, τ_{res}, (ps) for Water at 300 K as a Function of t^*

t^* (ps)	SPC/E	TIP4P	POL3
0	2.2	2.3	2.8
1	6.5	6.0	7.8
2	9.3	8.6	11
5	14	12	16
10	15	14	17

Dynamics. The interface residence time, τ_{res}, was calculated according to the procedure used by Impey et al.[73] and Smith and Dang to study ion hydration dynamics,[74] and later by Taylor et al. to study interface residence times of SPC/E.[75] The probability that a water molecule was located in the "90−10" region for a period of time longer than $(t - t_0)$ is given by

$$n(t - t_0) = \langle \sum_i P_i(t, t_0; t^*) \rangle$$

where $P_i(t, t_0; t^*) = 1$ if molecule i was at the interface at times t and t_0 and did not leave the interface for a continuous period of time longer than t^* in the time between. Otherwise, $P_i(t, t_0; t^*) = 0$. The brackets represent an average over the time origins t_0.

The normalized correlation functions were fit to a double exponential function of the form

$$n(t - t_0)/n(0) = A \exp(-(t - t_0)/\tau_A) + (1 - A) \exp(-(t - t_0)/\tau_B)$$

and τ_{res} was calculated from the fit parameters according to $\tau_{res} = A\tau_A + (1 - A)\tau_B$.

The values of τ_{res} for SPC/E, TIP4P, and POL3 with values of t^* varying from 0 to 10 ps are listed in Table 5 and are reasonably consistent for these three models. Because of the relatively short simulation times for the BLYP interaction potential, we could not compute a residence time with a reasonable precision.

With the information from the residence time calculation, the bulk and surface orientation dynamics were studied for SPC/E, TIP4P, POL3, and BLYP interaction potentials. The time correlation function for molecular reorientation was calculated according to

$$C_l(t - t_0) = \langle P_l [\hat{\mathbf{r}}(t - t_0) \cdot \hat{\mathbf{r}}(t_0); t^*] \rangle$$

where the brackets represent an average over time origins, t_0, and water molecules, P_l represents the lth Legendre polynomial, and $\hat{\mathbf{r}}$ is a unit vector along the relevant molecular direction. In this work, C_2 was calculated for the bisector of the H−O−H angle (electric dipole moment) if a water molecule was located in a region (interior or surface) at times t and t_0 and did not leave for a continuous period of time longer than t^* in the interim. Because the bulk water dipole reorientation is known to occur in approximately 4 ps and t^* must be shorter than this time to observe dynamics characteristic of a region, t^* was set equal to 1 ps. C_2 was calculated out to 6 ps because this is near τ_{res} with $t^* = 1$ ps. These times represented the compromise between capturing the dynamics of a region in a heterogeneous system and the finite lifetime of molecules in a region. Because we are only analyzing the last 4 ps of our BLYP trajectory, it is clear that our surface dynamics will not be able to be compared directly to those obtained via the classical empirical interaction potentials. However, it is still very instructive to make

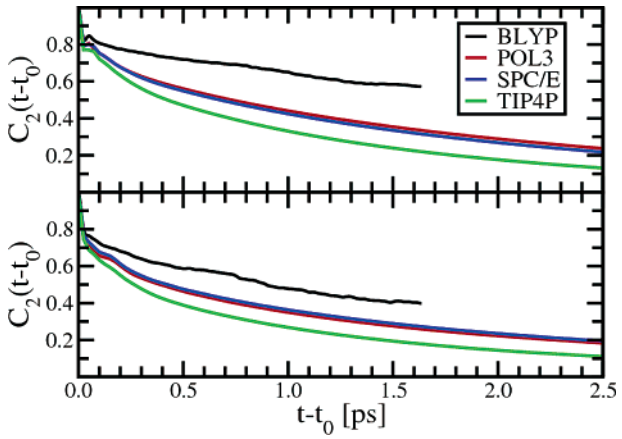

Figure 6. Rotational correlation for different water models in the interior (top) and surface regions (bottom).

an attempt to get a qualitative feeling for the differences. To this end, we analyze the last 4 ps of the ab initio MD simulations by defining the surface region to be within 2δ of the Gibbs dividing surface, whereas in the classical MD simulations, the surface will be defined within the "90−10" region. This should allow us to compensate for some diffusion across the "90−10" boundary and improve our statistics. The results are shown in Figure 6. The salient feature of this plot is that, in the interior region of the slab, the prominent librational feature of the short-time dynamics occurs at the same time. This is a very encouraging result, indicating that we indeed have a rotationally diffusing liquid in the interior region of the interfacial system, but relaxation is somewhat slower for BLYP compared to the empirical representations. Moreover, the rotational dynamics near the interface seem to be faster than the corresponding bulk for all models considered, again pointing to a consistent dynamical picture of the aqueous liquid−vapor interface independent of interaction potential used.

Conclusions

We have presented a comprehensive particle-based simulation study of the aqueous liquid−vapor interface. In particular, we have provided a comparison of classical empirical potentials (both fixed charge and polarizable) with an ab initio based interaction potential, namely BLYP, and compare our results to new experimental results that have been obtained for this important system. Our findings indicate that all structural and electronic properties are in close agreement. This is encouraging given the dramatic differences in the details of the interaction potential. In particular, the agreement of the surface populations of hydrogen bonded species seems to be independent of the precise nature of the interaction potential (e.g., polarizable or fixed charge). Of notable exception are the bulk density and the structural relaxation at the surface, where BLYP is the only description that significantly underestimates the bulk density, but is also the only model that yields an expansion of the oxygen−oxygen distance in the interfacial region. The more pronounced decrease in molecular dipole moment for BLYP near the surface when compared to other polarizable models such as FLUC-*q* and TIP4P−POL2 suggests that a dramatic loss of interaction energy due to charge reorganization occurred in the BLYP model. Thus, we have presented data that suggests that the expansion of BLYP water in the vicinity of the interface is most likely due to charge reorganization rather than relating to the short equilibration of our ab initio interfacial system. Furthermore, the inability for polarizable models such as FLUC-*q* and TIP4P−POL2 to capture the increase in the oxygen−oxygen distance near the surface suggests that interfacial properties must also be included as an additional training set in force field development. Thus, having established the existence of surface expansion for the BLYP interaction potential, the implications of this phenomena and its relation to the accommodation coefficients for water still need to be investigated.[6]

Acknowledgment. Part of this work was performed under the auspices of the U.S. Department of Energy (DOE) by the University of California LLNL under contract W-7405-ENG-48. Financial support from the National Science Foundation (CTS-0138393, CHE-0431312, and CHE-0209719), EMSI (ITR-0428774), and DOE Computational Science Graduate and 3M Foundation Fellowships (M.J.M.) is gratefully acknowledged. We thank R. Saykally, Jared Smith, Chris Cappa, and Nir Goldman for stimulating discussions, and the LLNL Computing staff for their help. Computer resources were provided by Livermore Computing, Minnesota Supercomputing Institute, and MPC Beowulf cluster at UCI.

References and Notes

(1) Ball, P. *Nature* **2003**, *423*, 25.
(2) Yaminsky, V.; Ohnishi, S. *Langmuir* **2003**, *19*, 1970.
(3) Steitz, R.; Gutberlet, T.; Hauss, T.; Klosgen, B.; Krastev, R.; Schemmel, S.; Simonsen, A. C.; Findenegg, G. H. *Langmuir* **2003**, *19*, 2409.
(4) Jensen, T. R.; Jensen, M. O.; Reitzel, N.; Balashev, K.; Peters, G. H.; Kjaer, K.; Bjornholm, T. *Phys. Rev. Lett.* **2003**, *9008*, 6101.
(5) Lum, K.; Chandler, D.; Weeks, J. D. *J. Phys. Chem. B* **1999**, *103*, 4570.
(6) Vieceli, J.; Roeselova, M.; Tobias, D. J. *Chem. Phys. Lett.* **2004**, *393*, 249.
(7) Chuang, P. Y.; Charlson, R. J.; Seinfeld, J. H. *Nature* **1997**, *390*, 594.
(8) Morita, A.; Sugiyama, M.; Kameda, H.; Koda, S.; Hanson, D. R. *J. Phys. Chem. B* **2004**, *108*, 9111.
(9) Knipping, E. M.; Lakin, M. J.; Foster, K. L.; Jungwirth, P.; Tobias, D. J.; Gerber, R. B.; Dabdub, D.; Finlayson-Pitts, B. J. *Science* **2000**, *288*, 301.
(10) Wilson, K. R.; Cavalleri, M.; Rude, B. S.; Schaller, R. D.; Catalano, T.; Nilsson, A.; Saykally, R. J.; Pettersson, L. G. M. *J. Phys. Chem. B* **2005**, *109*, 10194.
(11) Wilson, K. R.; Tobin, J. G.; Ankudinov, A. L.; Rehr, J. J.; Saykally, R. J. *Phys. Rev. Lett.* **2000**, *85*, 4289.
(12) Wilson, K. R.; Cavalleri, M.; Rude, B. S.; Schaller, R. D.; Nilsson, A.; Pettersson, L. G. M.; Goldman, N.; Catalano, T.; Bozek, J. D.; Saykally, R. J. *J. Phys. Condens. Mater.* **2002**, *14*, L221.
(13) Wilson, K. R.; Schaller, R. D.; Co, D. T.; Saykally, R. J.; Rude, B. S.; Catalano, T.; Bozek, J. D. *J. Chem. Phys.* **2002**, *117*, 7738.
(14) Wilson, K. R.; Rude, B. S.; Catalano, T.; Schaller, R. D.; Tobin, J. G.; Co, D. T.; Saykally, R. J. *J. Phys. Chem. B* **2001**, *105*, 3346.
(15) Richmond, G. L. *Chem. Rev.* **2002**, *102*, 2693.
(16) Raymond, E. A.; Richmond, G. L. *J. Phys. Chem. B* **2004**, *108*, 5051.
(17) Raymond, E. A.; Tarbuck, T. L.; Brown, M. G.; Richmond, G. L. *J. Phys. Chem. B* **2003**, *107*, 546.
(18) Allen, H. C.; Raymond, E. A.; Richmond, G. L. *Curr. Opin. Colloid Interface Sci.* **2000**, *5*, 74.
(19) Du, Q.; Superfine, R.; Freysz, E.; Shen, Y. R. *Phys. Rev. Lett.* **1993**, *70*, 2313.
(20) Schnitzer, C.; Baldelli, S.; Campbell, D. J.; Shultz, M. J. *J. Phys. Chem. A* **1999**, *103*, 6383.
(21) Schnitzer, C.; Baldelli, S.; Shultz, M. J. *J. Phys. Chem. B* **2000**, *104*, 585.
(22) Liu, D. F.; Ma, G.; Levering, L. M.; Allen, H. C. *J. Phys. Chem. B* **2004**, *108*, 2252.
(23) Wernet, P.; Nordlund, D.; Bergmann, U.; Cavalleri, M.; Odelius, M.; Ogasawara, H.; Naslund, L. A.; Hirsch, T. K.; Ojamae, L.; Glatzel, P.; Pettersson, L. G. M.; Nilsson, A. *Science* **2004**, *304*, 995.
(24) Smith, J. D.; Cappa, C. D.; Wilson, K. R.; Messer, B. M.; Cohen, R. C.; Saykally, R. J. *Science* **2004**, *306*, 851.
(25) Schnitzer, C.; Baldelli, S.; Shultz, M. J. *Chem. Phys. Lett.* **1999**, *313*, 416.
(26) Townsend, R. M.; Gryko, J.; Rice, S. A. *J. Chem. Phys.* **1985**, *82*, 4391.

(27) Townsend, R. M.; Rice, S. A. *J. Chem. Phys.* **1991**, *94*, 2207.
(28) Wilson, M. A.; Pohorille, A.; Pratt, L. R. *J. Phys. Chem.* **1987**, *91*, 4873.
(29) Benjamin, I. *J. Chem. Phys.* **1991**, *95*, 3698.
(30) Benjamin, I. *Phys. Rev. Lett.* **1994**, *73*, 2083.
(31) Rick, S. W.; Stuart, S. J.; Berne, B. J. *J. Chem. Phys.* **1994**, *101*, 6141.
(32) Chen, B.; Xing, J. H.; Siepmann, J. I. *J. Phys. Chem. B* **2000**, *104*, 2391.
(33) Dang, L. X.; Chang, T. M. *J. Chem. Phys.* **1997**, *106*, 8149.
(34) Car, R.; Parrinello, M. *Phys. Rev. Lett.* **1985**, *55*, 2471.
(35) Marx, D.; Hutter, J. Ab Initio Molecular Dynamics: Theory and Implementation. In *Modern Methods and Algorithms of Quantum Chemistry*; Grotendorst, J., Ed.; John von Neumann Institute for Computing: Forschungszentrum Juelich: Juelich, 2000; Vol. 1, p 301.
(36) Vassilev, P.; Hartnig, C.; Koper, M. T. M.; Frechard, F.; van Santen, R. A. *J. Chem. Phys.* **2001**, *115*, 9815.
(37) *CPMD*, 3.9 ed.; IBM Corporation: White Plains, NY, 1990−2001; MPI fur Festkorperforschung Stuttgart: Stuttgart, 1997−2005.
(38) Kuo, I. F. W.; Mundy, C. J. *Science* **2004**, *303*, 658.
(39) Panagiotopoulos, A. Z. *Mol. Phys.* **1987**, *61*, 813.
(40) Panagiotopoulos, A. Z.; Quirke, N.; Stapleton, M.; Tildesley, D. J. *Mol. Phys.* **1988**, *63*, 527.
(41) Berendsen, H. J. C.; Grigera, J. R.; Straatsma, T. P. *J. Chem. Phys.* **1987**, *91*, 6269.
(42) Jorgensen, W. L.; Chandrasekhar, J.; Madura, J.; Impey, R. W.; Klein, M. L. *J. Chem. Phys.* **1983**, *79*, 926.
(43) Caldwell, J. W.; Kollman, P. A. *J. Phys. Chem.* **1995**, *99*, 6208.
(44) Hura, G.; Russo, D.; Glaeser, R. M.; Head-Gordon, T.; Krack, M.; Parrinello, M. *Phys. Chem. Chem. Phys.* **2003**, *5*, 1981.
(45) *CPMD*; http://www.cpmd.org.
(46) Mortensen, J. J.; Parrinello, M. *J. Phys. Chem. B* **2000**, *104*, 2901.
(47) Becke, A. D. *Phys. Rev. A* **1988**, *38*, 3098.
(48) Lee, C.; Yang, W.; Parr, R. G. *Phys. Rev. B* **1988**, *37*, 785.
(49) Troullier, N.; Martins, J. L. *Phys. Rev. B* **1991**, *43*, 1993.
(50) Hoover, W. G. *Phys. Rev. A* **1985**, *31*, 1695.
(51) Nose, S. *J. Chem. Phys.* **1984**, *81*, 511.
(52) Kuo, I. F. W.; Mundy, C. J.; McGrath, M. J.; Siepmann, J. I.; VandeVondele, J.; Sprik, M.; Hutter, J.; Chen, B.; Klein, M. L.; Mohamed, F.; Krack, M.; Parrinello, M. *J. Phys. Chem. B* **2004**, *108*, 12990.
(53) Lippert, G.; Hutter, J.; Parrinello, M. *Mol. Phys.* **1997**, *92*, 477.
(54) VandeVondele, J.; Krack, M.; Mohamed, F.; Parrinello, M.; Chassaing, T.; Hutter, J. *Comput. Phys. Commun.* **2005**, *167*, 103.
(55) *CP2K*; http://cp2k.berlios.de.
(56) Goedecker, S.; Teter, M.; Hutter, J. *Phys. Rev. B* **1996**, *54*, 1703.
(57) Krack, M.; Parrinello, M. Quickstep: Make the Atoms Dance. In *High Performance Computing in Chemistry*; Grotendorst, J., Ed.; John von Neumann Institute for Computing, Forschungszentrum Juelich: Juelich, 2004; Vol. 25, p 29.
(58) Darden, T.; York, D.; Pedersen, L. *J. Chem. Phys.* **1993**, *98*, 10089.
(59) Ryckaert, J. P.; Ciccotti, G.; Berendsen, H. J. C. *J. Comput. Chem.* **1977**, *23*, 327.
(60) Pearlman, D. A.; Case, D. A.; Caldwell, J. W.; Ross, W. S.; Cheatham, T. E.; Debolt, S.; Ferguson, D.; Seibel, G.; Kollman, P. *Comput. Phys. Commun.* **1995**, *91*, 1.
(61) Siepmann, J. I.; Frenkel, D. *Mol. Phys.* **1992**, *75*, 59.
(62) Martin, M. G.; Siepmann, J. I. *J. Phys. Chem. B* **1999**, *103*, 4508.
(63) Chen, B.; Siepmann, J. I.; Klein, M. L. *J. Am. Chem. Soc.* **2002**, *124*, 12232.
(64) McGrath, M. J.; Siepmann, J. I.; Kuo, I. F. W.; Mundy, C. J.; VandeVondele, J.; Hutter, J.; Mohamed, F.; Krack, M. *ChemPhysChem* **2005**, *6*, 1894.
(65) McGrath, M. J.; Siepmann, J. I.; Kuo, I. F. W.; Mundy, C. J.; VandeVondele, J.; Sprik, M.; Hutter, J.; Mohamed, F.; Krack, M.; Parrinello, M. *Comput. Phys. Commun.* **2005**, *169*, 289.
(66) McGrath, M. J.; Siepmann, J. I.; Kuo, I. F. W.; Mundy, C. J.; VandeVondele, J.; Hutter, J.; Mohamed, F.; Krack, M. *J. Phys. Chem. A* **2005**, ASAP September 21, 2005, http://dx.doi.org/10.1021/jp0535947.
(67) Berghold, G.; Mundy, C. J.; Romero, A. H.; Hutter, J.; Parrinello, M. *Phys. Rev. B* **2000**, *61*, 10040.
(68) Silvestrelli, P. L.; Parrinello, M. *Phys. Rev. Lett.* **1999**, *82*, 3308.
(69) Silvestrelli, P. L.; Parrinello, M. *J. Chem. Phys.* **1999**, *111*, 3572.
(70) Perry, A.; Niepert, C.; Ridley, C.; Space, B.; Moore, P. *Phys. Rev. E* **2005**, *71*, 050601(R).
(71) Harpaz, Y.; Gerstein, M.; Chothia, C. *Structure* **1994**, *2*, 641.
(72) Gerstein, M.; Tsai, J.; Levitt, M. *J. Mol. Biol.* **1995**, *249*, 955.
(73) Impey, R. W.; Madden, P. A.; McDonald, I. R. *J. Phys. Chem.* **1983**, *87*, 5071.
(74) Smith, D. E.; Dang, L. X. *J. Chem. Phys.* **1994**, *100*, 3757.
(75) Taylor, R. S.; Dang, L. X.; Garrett, B. C. *J. Phys. Chem.* **1996**, *100*, 11720.